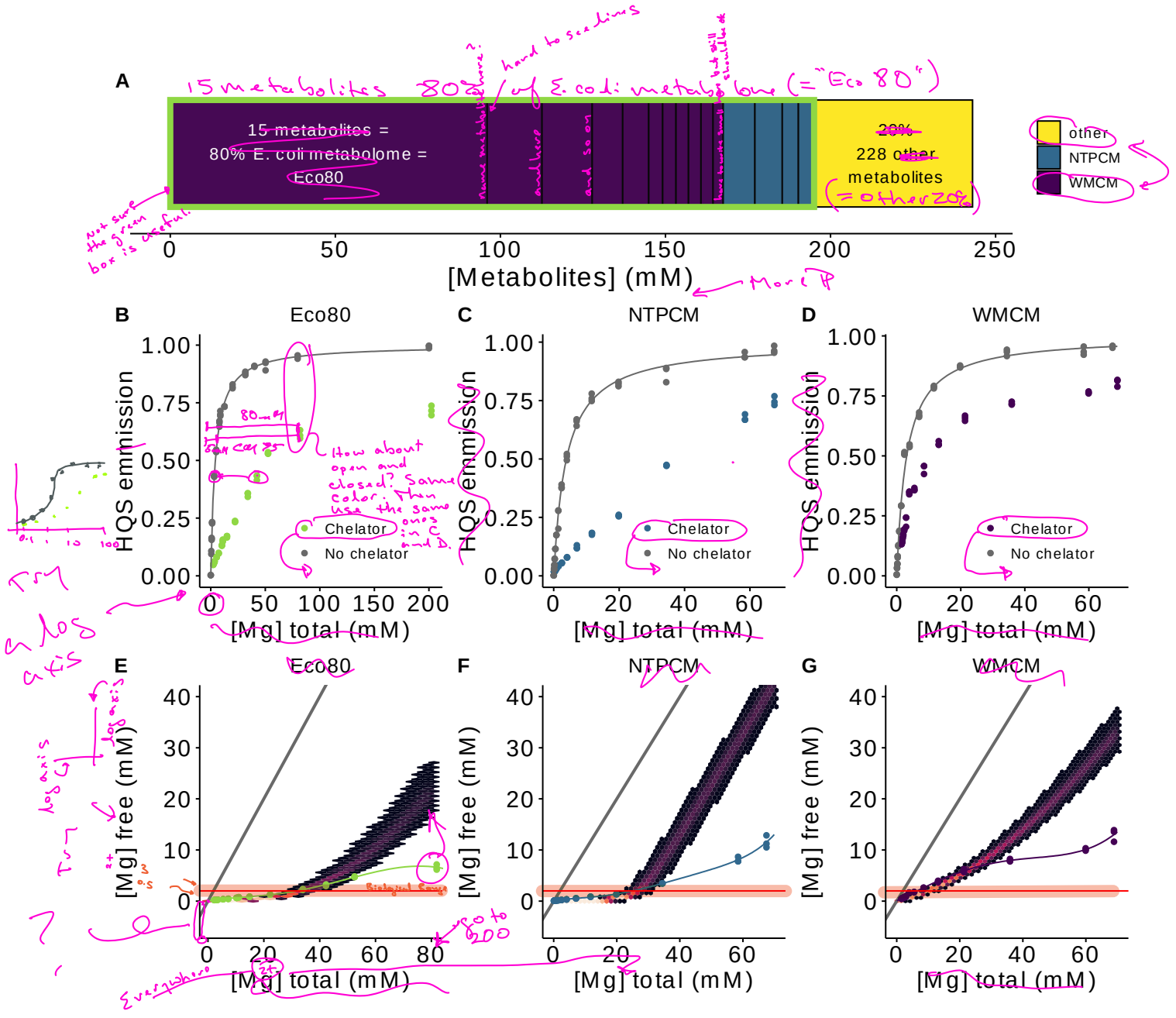

Figure 1 Analysis of Mg^{2+} speciation in *E. coli* metabolite mixtures. Eco80 contains **(A)** E. coli metabolome molar composition. Eco80 contains the 15 most abundant metabolites that compose 80% of the *E. coli* metabolome. NTPCM contains four strong Mg^{2+} chelating NTPs, and WMCM contains 11 other weak $Mg^{2+\ binding}$ metabolites **(B-D)** Effect of Mg^{2+} on 8-hydroxyquinoline-5-sulphonic acid (HQS) emission with and without mixtures of metabolites that chelate Mg^{2+}. Grey lines represent fits to determine the binding constant for Mg^{2+} and HQS. **(E-G)** Effect of the total Mg^{2+} concentration on the free Mg^{2+} concentration with mixtures of metabolites that chelate Mg^{2+}. Free Mg^{2+} was calculated using HQS emission and the binding constant for Mg^{2+} and HQS. Grey lines represent the free Mg^{2+} concentration in the absence of chelators (free Mg^{2+} = total Mg^{2+}). Hex bins represent a statistical simulation of 1000 virtual artificial cytoplasms based on experimental errors in K_D determination, experimental errors in reagent concentrations, and single site binding.

Table 1. Eco80: the top 15 most abundant metabolites that comprise 80% of the *E. coli* metabolome.

Metabolite	Conc. (mM)	K_D (mM)	Chelation stength
ATP	9.63	0.28 (0.01)[a]	NTPCM (Strong[d])
UTP	8.29	0.248 (0.004)[a]	NTPCM (Strong[d])
GTP	4.87	0.201 (0.007)[a]	NTPCM (Strong[d])
dTTP	4.62	0.160 (0.003)[a]	NTPCM (Strong[d])
L-Glutamic acid	96	520 (50)[b]	WMCM (Weak[d])
Glutathione	16.6	NA[c]	WMCM (Weak[d])
Fructose 1,6-bisphosphate	15.2	5.9 (0.1)[a]	WMCM (Weak[d])
UDP-N-acytylglucosamine	9.24	29 (2)[a]	WMCM (Weak[d])
Glucose 6-phosphate	7.88	17.3 (0.2)[a]	WMCM (Weak[d])
L-Aspartic acid	4.23	465 (12)[b]	WMCM (Weak[d])
L-Valine	4.02	NA[c]	WMCM (Weak[d])
L-Glutamine	3.81	NA[c]	WMCM (Weak[d])
6-Phospho-gluconic acid	3.77	14.4 (0.2)[a]	WMCM (Weak[d]
Pyruvic acid	3.66	3.6 (0.9)[b]	WMCM (Weak[d])
Dihydroxyacetone phosphate	3.06	20 (1)[a]	WMCM (Weak[d])

[a]Determined at 37 °C with Isothermal titration calorimetry. Error is the propagated standard error in the fit parameters.
[b]Determined at 37 °C with HQS emission Error is the propagated standard error in the fit parameters.
[c]No binding observed as per SI Figure 2
[d]Metabolites with KDs for Mg^{2+} less than 2 mM are considered strong Mg^{2+} chelators.

S?
which
Remove gray
Squeeze it done
as measured (Fig SI?) herein
OK to leave this many sig figs if original paper reported them.

SI Table 1. Recipe for the Eco80 artificial cytoplasm (Add in later in word when I am formatting the tables)

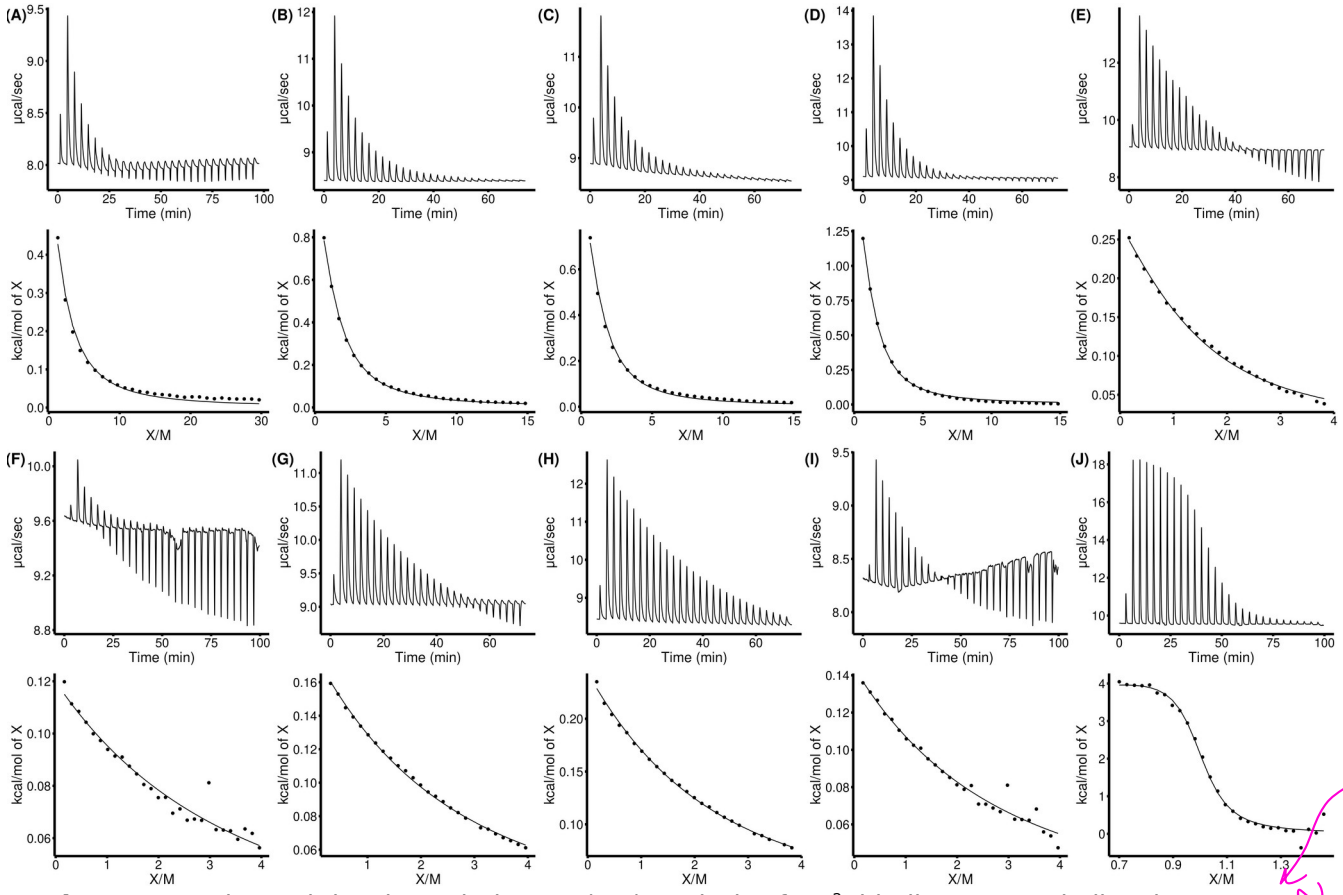

SI Figure 1 Isothermal titration calorimetry (ITC) analysis of Mg^{2+} binding to metabolites in ~~240 mM~~ NaCl 140 mM KCl 10 mM HEPES pH 7.0 at 37 °C. $MgCl_2$ was titrated into metabolites and the power was monitored over time (Top panel). Heat of the injection was calculated by integrating the raw power curve, and the background heat of $MgCl_2$ diltution, collected on buffer containing no metabolite, was subtracted to produce the isotherms in the bottom panels. Lines in bottom pannels represent fits to the Weismann isotherm equation to determine apparent association constants. **(A)** Adenosine triphosphate (ATP). **(B)** Uridine triphosphosphate (UTP). **(C)** Guanosine triphsophate (GTP). **(D)** deoythymidine triphosphate (dTTP). **(E)** Fructose 1,6-bisphosphate. **(F)** Uridine diphosphate (UDP)-N-acytylglucosamine. **(G)** Glucose 6-phosphate. **(G)** 6-phosphogluconic acid. **(H)** phosphoenol pyruvate. **(G)** Ethylene diamine-tetracetic acid (EDTA).

SI Table 2 Apparent binding constants determined with Isothermal titration calorimetry (ITC).

Metabolite	Syringe (mM)	Cell (mM)	ΔH (kcal/mol)	K' (M^{-1})	K_D' (mM^{-1})
ATP	15 mM $MgCl_2$[a]	0.1 mM ATP[a]	1.83 (0.04)	3600 (200)	0.28 (0.01)
UTP	15 mM $MgCl_2$[a]	0.2 mM UTP[a]	1.70 (0.01)	4200 (70)	0.248 (0.004)
GTP	15 mM $MgCl_2$[a]	0.2 mM GTP[a]	1.43 (0.02)	5000 (200)	0.201 (0.007)
dTTP	15 mM $MgCl_2$[a]	0.2 mM dTTP[a]	2.19 (0.02)	6300 (300)	0.160 (0.003)
Fructose 1,6-BP	100 mM $MgCl_2$[a]	5.0 mM Fructose 1,6-BP[a]	0.414 (0.004)	169 (4)	5.9 (0.1)
UDP-GlcNAC	100 mM $MgCl_2$[a]	5.0 mM UDP-GlcNAC	0.57 (0.02)	34 (2)	29 (2)
Glucose 6-P	100 mM $MgCl_2$[a]	5.0 mM Glucose 6-P[a]	0.555 (0.003)	57.9 (0.7)	17.3 (0.2)
6-P-gluconic acid	100 mM $MgCl_2$[a]	5.0 mM 6-P-gluconic acid[a]	0.662 (0.005)	70 (1)	14.4 (0.2)
Dihydroxyacetone phosphate	100 mM $MgCl_2$[a]	5.0 mM dihydroxy-acetone phosphate[a]	0.50 (0.01)	51 (3)	20 (1)
EDTA	6 mM $MgCl_2$[a]	1.5 mM EDTA 1.0 mM $MgCl_2$[a,b]	2.85 (0.04)	220,000 (30,000)	0.0045 (0.0006)

[a]240 mM NaCl 140 mM KCl 10 mM HEPES pH 7.0 at 37 °C

[b]Mg^{2+} and EDTA were incorporated into the cell in order to sequester trace tight binding metal ions and thereby negate their contribution to ITC signal.

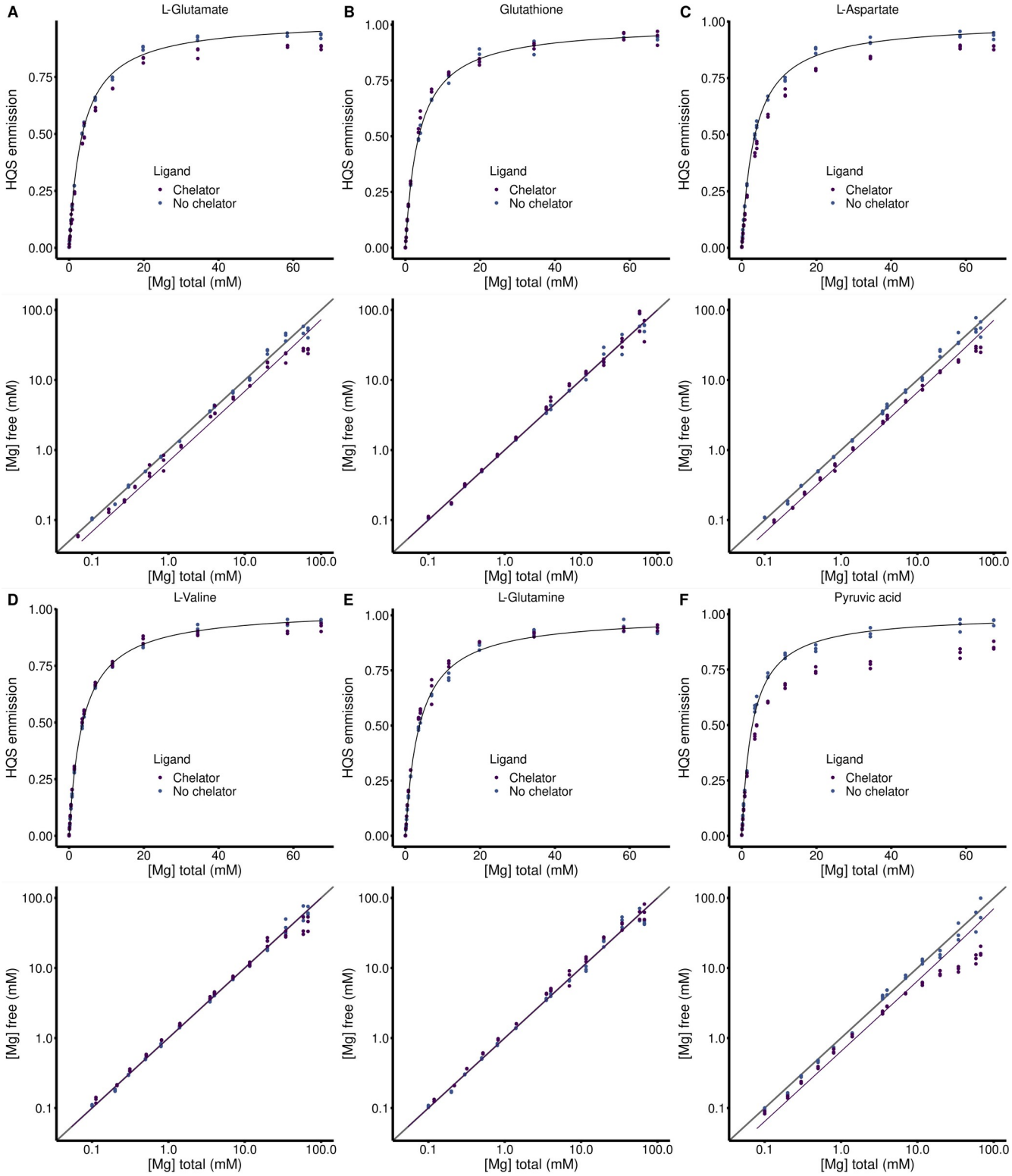

SI Figure 2 HQS analysis of Mg2+ binding to metabolites in 240 mM NaCl 140 mM KCl 20 mM MOPS 0.01 mM EDTA 0.001% SDS pH 7.0. (Top panels) Dependence of HQS emission on the total concentration of $MgCl_2$ in the presence and absence of a metabolite chelators. Black lines represent a fit to SI equation 1 to determine the F_{max}, F_{min}, and K_{HQS}. (Bottom panels) Dependence of the free Mg^{2+} concentration on the total concentration of $MgCl_2$ in the presence and absence of a metabolite chelators. Grey lines represent where the free Mg^{2+} concentration equals the total concentration of $MgCl_2$, Purple lines represent a fit to SI equation 4 to determine the association constant between HQS and a chelator. **(A)**

240 mM L-glutamate. **(B)** 194 Glutathione. **(C)** 240 mM L-aspartate. **(D)** 240 mM L-valine. **(E)** 240 mM L-glutamine. **(F)** 5 mM pyruvic acid.

SI Table 3 Apparent binding constants determined with HQS emission. F_{max}, F_{min}, and K_{HQS} are determined by fitting HQS emission in the absence of chelators and used to calculate the free Mg^{2+} concentration in each sample. Metabolite binding constants, K' and K_D'. are determined by fitting the relationship between the free Mg^{2+} concentration and the total $MgCl_2$ concentration using SI Equation 4.

Metabolite	F_{max}	F_{min}	K_{HQS} (mM^{-1})	K' (mM^{-1})	K_D' (mM^{-1})
L-Glutamic acid	187,000 (1000)	0 (810)	0.281 (0.008)	0.0019 (0.0002)	520 (50)
Glutathione	182,000 (1000)	592 (750)	0.279 (0.007)	NA[c]	NA[c]
L-Aspartic acid	196,000 (1000)	0 (820)	0.283 (0.007)	0.0021 (0.0001)	465 (12)
L-Valine	188,200 (800)	495 (580)	0.274 (0.005)	NA[c]	NA[c]
L-Glutamine	190,000 (1400)	516 (110)	0.27 (0.01)	NA[c]	NA[c]
Pyruvic acid	188,000 (1500)	0 (1300)	0.35 (0.01)	0.28 (0.07)	3.6 (0.9)

[c]No binding observed as per SI Figure 2

SI Table 3. HQS fits in the absence of chelators, used to determine free Mg2+ concentrations. F_{max}, F_{min}, and K_{HQS} are determined by fitting HQS emission in the absence of chelators and used to calculate the free Mg^{2+} concentration in each sample.

Metabolite	F_{max}	F_{min}	K_{HQS} (mM^{-1})
Eco80	185,100 (800)	124 (1000)	0.239 (0.005)
NTPCM	187,000 (1500)	436 (1000)	0.26 (0.01)
WMCM	179,000 (1600)	0 (1400)	0.32 (0.01)

Table 2. Total Mg^{2+} concentrations used to obtain 2 mM free Mg^{2+} in artificial cytoplasms.

Condition	Total [Mg^{2+}] (mM)	Chelated [Mg^{2+}] (mM)	Free [Mg^{2+}] (mM)
Eco80	31.6	29.6	2.0
NTPCM	25.0	23	2.0
WMCM	6.4	4.5	2.0

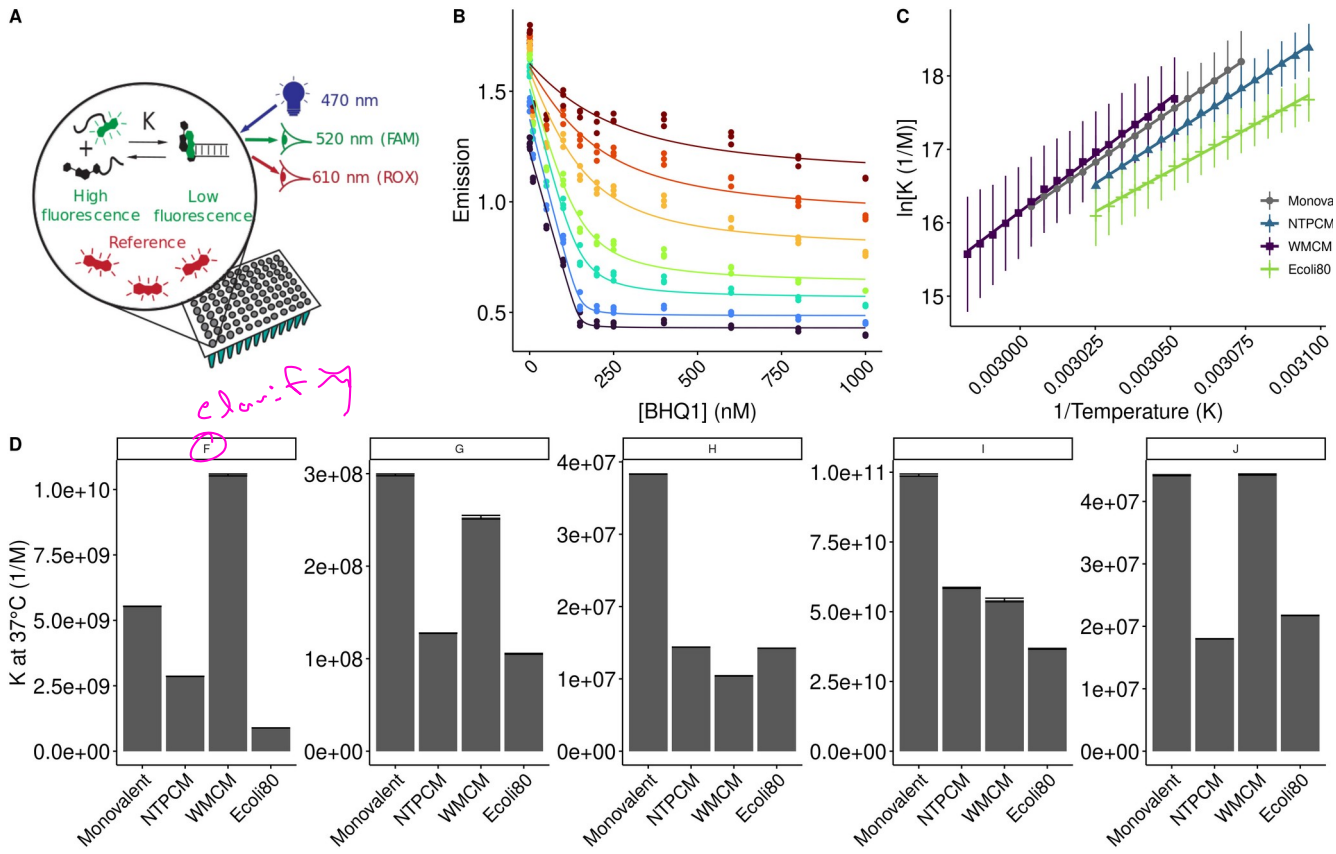

Figure 2 *E. coli* metabolite and Mg^{2+} mixtures destabilize RNA secondary structure.

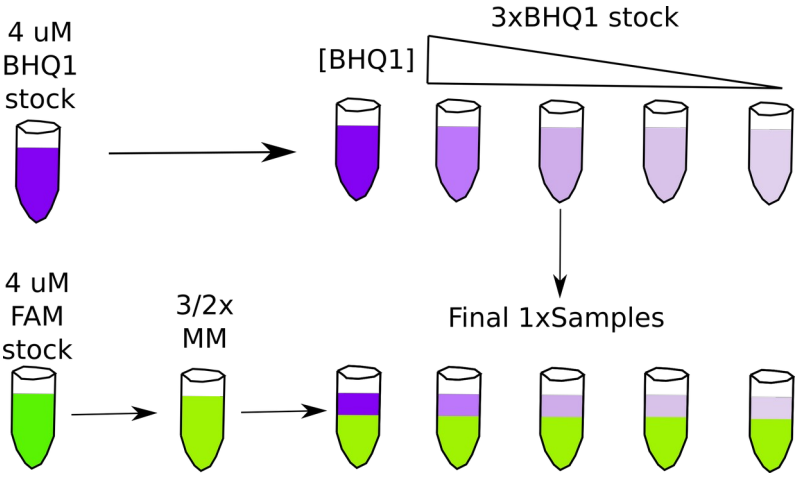

SI figure 3 *E. coli* metabolite and Mg^{2+} mixtures destabilize RNA secondary structure.

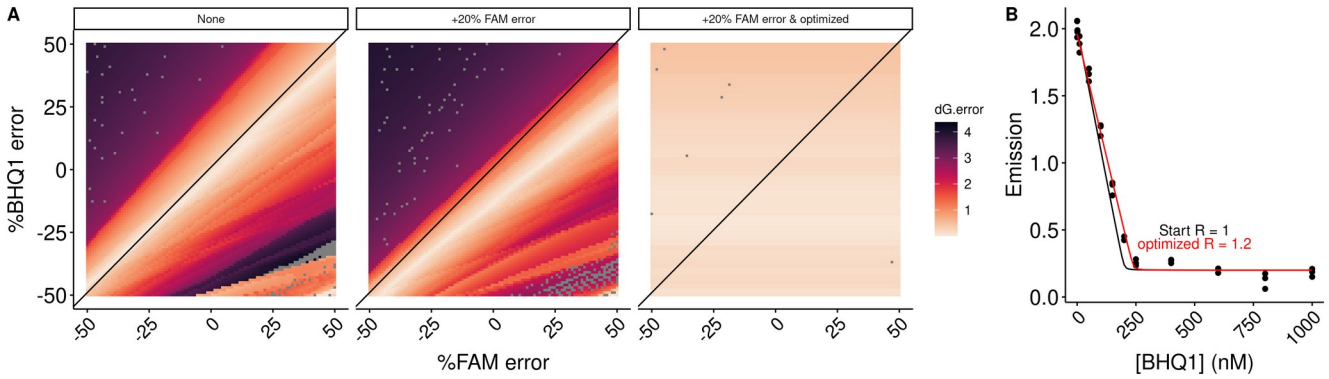

SI figure 4 *E. coli* metabolite and Mg^{2+} mixtures destabilize RNA secondary structure.

Table 3. Stability of RNA helices in *E. coli* metabolite mixtures.

Helix	Sequence (5'-FAM/ BHQ1-3')	AU content	Condition	dH (kcal/mol)	dS (cal/mol/K)	dG (kcal/mol)	ddG (kcal/mol)
F	CGCAUCCU/ AGGAUGCG	0.38	2 mM free	-55.9 (0.2)	-136.0 (0.7)	-13.82 (0.01)	
			NTPCM	-52.2 (0.4)	-125 (1)	-13.41 (0.02)	0.41 (0.02)
			WMCM	-61.4 (0.8)	-152 (2)	-14.22 (0.05)	-0.40 (0.05)
			Ecoli80	-44.5 (0.7)	-102 (2)	-12.70 (0.04)	1.13 (0.04)
G	CCAUAUCA/ UGAUAUGG	0.63	2 mM free	-53.4 (1.0)	-133 (3)	-12.02 (0.04)	
			NTPCM	-42.9 (0.5)	-101 (1)	-11.50 (0.02)	0.52 (0.04)
			WMCM	-53 (2)	-132 (7)	-11.9 (0.1)	0.10 (0.01)
			Ecoli80	-57 (2)	-146 (5)	-11.38 (0.05)	0.64 (0.06)
H	CCAUAUUA/ UAAUAUGG	0.75	2 mM free	-53.5 (0.4)	-137 (1)	-10.76 (0.01)	
			NTPCM	-45.0 (0.2)	-112.5 (0.5)	-10.158 (0.002)	0.60 (0.01)
			WMCM	-43 (2)	-107 (5)	-9.94 (0.02)	0.80 (0.02)
			Ecoli80	-41.3 (0.2)	-100.4 (0.7)	-10.15 (0.01)	0.61 (0.01)
I	CGGAUGGC/ GCCAUCCG	0.25	2 mM free	-71.1 (0.8)	-179 (2)	-15.6 (0.06)	
			NTPCM	-70.4 (0.6)	-177 (2)	-15.28 (0.05)	0.32 (0.08)
			WMCM	-65.5 (2)	-162 (7)	-15.2 (0.2)	0.4 (0.2)
			Ecoli80	-69.7 (0.8)	-176 (3)	-14.0 (0.1)	0.61 (0.08)
J	CGUAUGUA/ UACAUACG	0.63	2 mM free	-63.2 (0.9)	-169 (3)	-10.85 (0.02)	
			NTPCM	-59 (1)	-157 (4)	-10.30 (0.01)	0.55 (0.02)
			WMCM	-67 (1)	-180 (3)	-10.85 (0.02)	0.00 (0.03)
			Ecoli80	-61 (1)	-164 (3)	-10.41 (0.01)	0.44 (0.02)

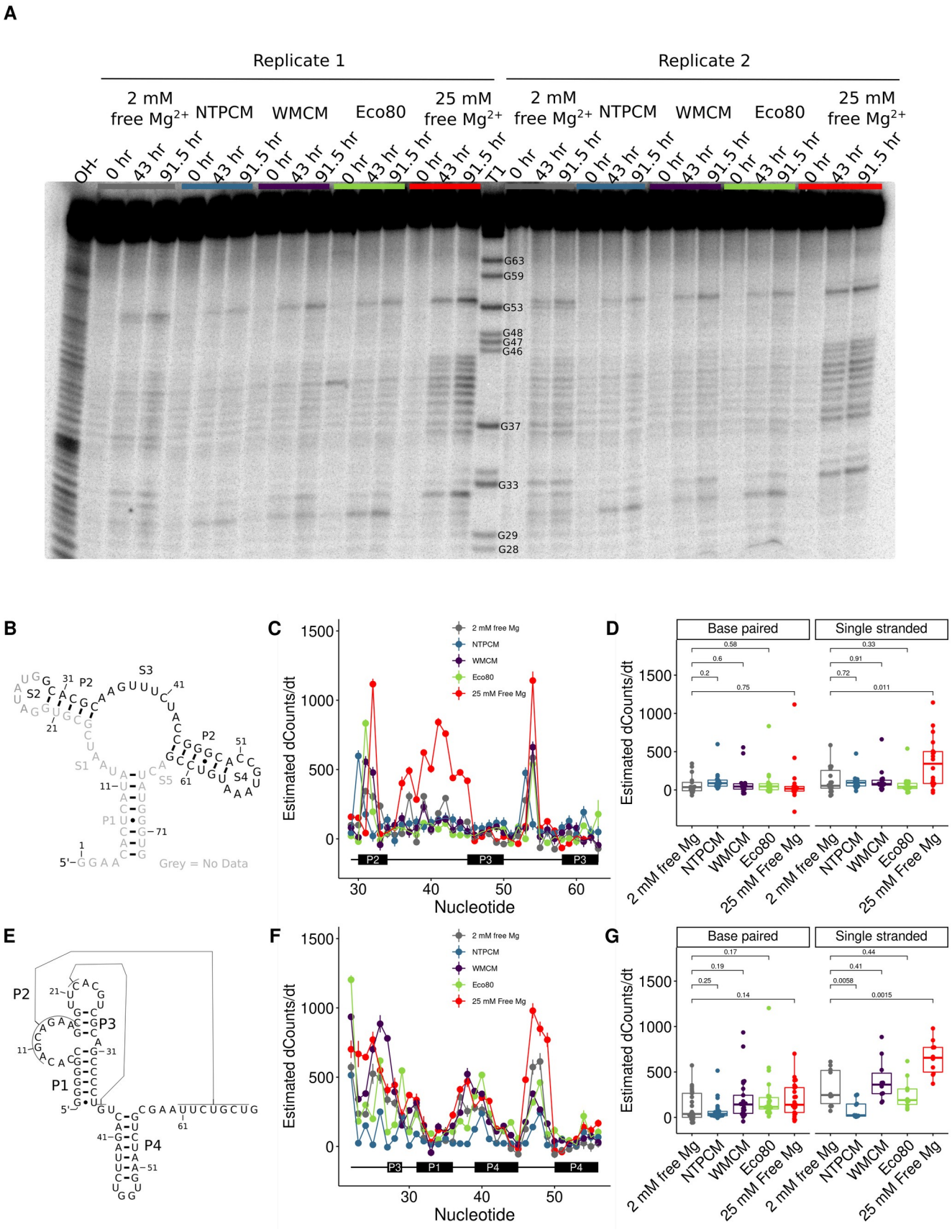
A
Replicate 1
Replicate 2
2 mM free Mg2+
NTPCM
WMCM
Eco80
25 mM free Mg2+
OH-
0 hr
43 hr
91.5 hr
T1
G63
G59
G53
G48
G47
G46
G37
G33
G29
G28
B
S3
P2
S1
S2
S4
S5
P1
P3
P4
Grey = No Data
C
Estimated dCounts/dt
Nucleotide
2 mM free Mg
NTPCM
WMCM
Eco80
25 mM Free Mg
D
Base paired
Single stranded
Estimated dCounts/dt
E
F
G

Figure 3 *E. coli* metabolite and Mg^{2+} mixtures stabilize the chemical structure of RNA. **(A)** Raw degradation assay gel image for the Guanine riboswitch aptamer incubated in artificial cytoplasms at 37 °C and pH 7. The OH- lane contains a hydrolysis ladder which cleaves after every nucleotide and T1 contains the RNA treated with T1 ribonuclease which cleaves after every G. Enough Mg^{2+} was added to each artificial cytoplasm to have 2 mM Mg^{2+} as determined in Figure 1. **(B)** Secondary structure of the guanine riboswitch aptamer. **(C)** Estimated increase in counts as a function of time at each residue in different solution conditions as a function of location in the RNA. **(D)** Estimated increase in counts as a function of time in different conditions grouped by paired and unpaired bases. Significance was determined using a student's t-test. **(E)** Secondary structure of the cleaved human CPEB3 HDV ribozyme. **(C)** Estimated increase in counts as a function of time at each residue in different solution conditions as a function of location in the RNA. **(D)** Estimated increase in counts as a function of time in different conditions grouped by paired and unpaired bases. Significance was determined using a student's t-test.

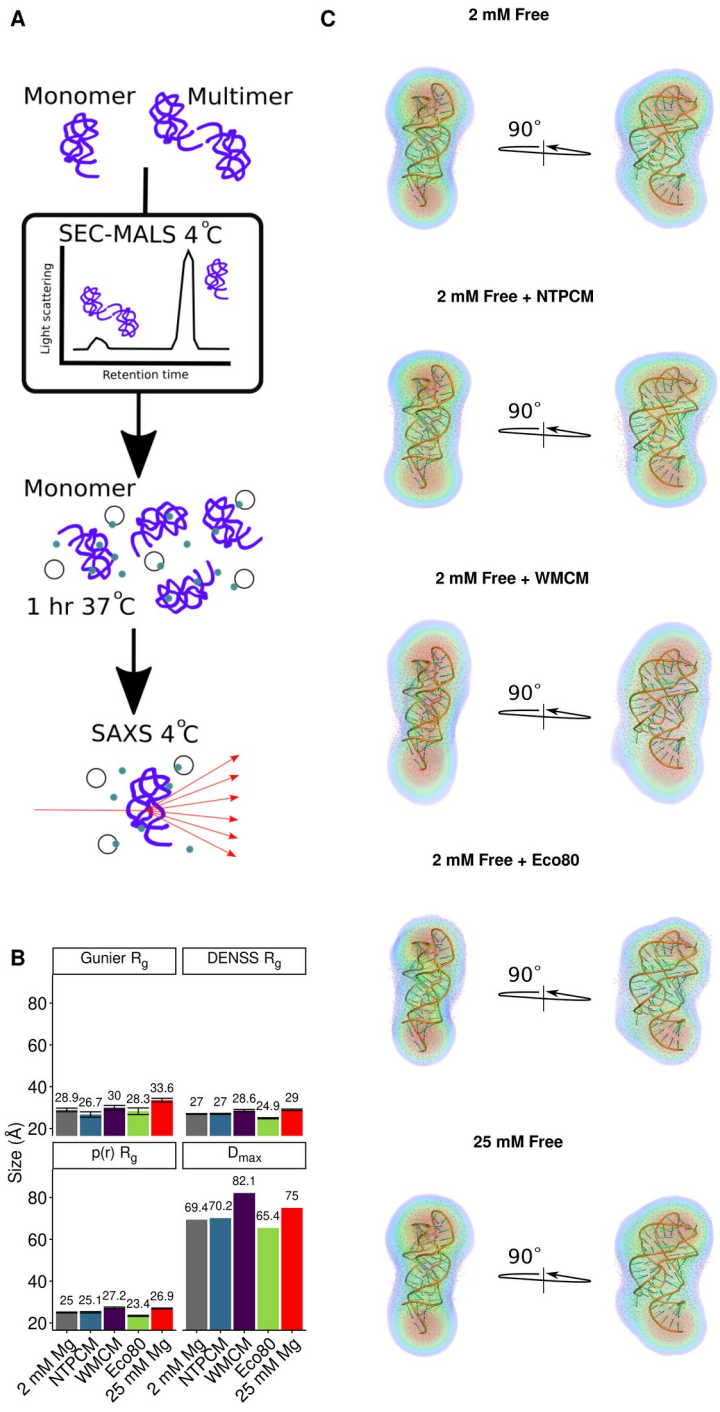

Figure 4 *E. coli* metabolite and Mg^{2+} mixtures increase functional RNA compactness.

ABSTRACT: Herein, we examine the complicated network of interactions among RNA, the metabolome, and the metalome in conditions that mimic the *E. coli* cytoplasm. First, we determined Mg^{2+} binding constants for the top 15 *E. coli* metabolites, comprising 80% of the total metabolome, at physiological pH and monovalent ion concentrations. Then, we used this information to inform creation of artificial cytoplasms that mimic *in vivo E. coli* conditions, termed Eco80. We empirically determined that the mixture of *E. coli* metabolites in Eco80 approximates single sit binding behavior towards Mg2+ in the biologically relevant free Mg2+ range of ~0.5 to 3 mM Mg^{2+}, using a Mg^{2+} binding fluorescent dye (8-Hydroxy-5-quinolinesulfonic acid). Furthermore, we examined the effects of Eco80 conditions on the thermodynamic stability, chemical stability, catalysis, and compactness of RNA. We find that these Eco80 conditions lead to opposing effects, wherein thermodynamic stability of RNA helices were weakened but chemical stability, compactness, and catalysis were enhanced. We propose a mechanism where increased RNA compactness and catalysis is facilitated in Eco80.

Introduction

Summary of progress on in vivo-like conditions.

Studies that consider cellular components one at a time.

Studies that consider cellular components together in artificial cytoplasm.

In contrast, we take a bottom up, *aufbau*, approach that builds up complexity, to make an artificial cytoplasm that contains 80% of *E. coli* metabolites with biologically relavent concentrations of monovalent ions and free Mg^{2+} ions. This *aufbau* approach allows us to understand the effects of 80% of metabolite and metal ion species that compose the network of interactions that RNA experiences in *E. coli* cells.

Eco80: A artificial cytoplasm containing 80% of *E. coli* metabolites

E. coli cells contain hundreds of metabolites (about 243 mM total), which is too many metabolites to test systematically. However, 15 abundant metabolites, an experimentally manageable number, comprise 80% (195 mM) of total metabolites (Figure 1A). Thus, we sought to prepare Eco80, an artificial cytoplasm containing the biological concentrations of the 15 most abundant metabolites in *E. coli* (Table 1).

All of the metabolites in Eco80 are zwitter ions or negatively charged near physiological pH (~7) and require electrostatic neutralization with metal ions. Thus, we prepared Eco80 so that the final monovalent ion concentration was the physiological value of 240 mM Na^+ and 140 mM K^+ (Supplementary information (SI) Table 1). Metabolite salts and free acids were prepared to a final 2xconcentration, and the amount of Na^+ and K^+ added with each metabolite was recorded. Next, the pH of the 2xstock was adjusted to pH 7.0 using NaOH, and the amount of Na^+ was recorded. Lastly, NaCl and KCl was added to a final 240 mM Na^+ and 140 mM K^+. We thus created Eco80, at a 2x final concentration so that it could be diluted into other reagents for experiments.

Next, we considered how metabolites effect the speciation of free and chelated Mg^{2+}. All 15 Eco80 metabolites have functional groups, carboxylates and phosphates, that drive chelating interactions with divalent Mg^{2+} ions (Table 1), and we have previously estimated that the metabolite pool in *E. coli* has potential to chelate 51 mM Mg^{2+}, assuming 2 mM free Mg^{2+}, at an ionic strength of 0.15 M and a pH of 7.5. While extensive literature exists on chelating interactions between Mg^{2+} and small molecules, our previous estimates are putative as Mg^{2+} chelation strength is dependent on environmental factors such as pH, ionic strength, the composition of background ions, and temperature. Thus, we sought to better characterize Mg^{2+} chelation by the metabolites in Eco80, at the physiological background of 240 mM Na^+, 140 mM K^+, pH 7.0, and 37 °C.

We determined apparent disassociation constants (K_D) for Eco80 metabolites in 240 mM NaCl, 140 mM KCl, pH 7.0 buffer at 37 °C (Table 1). Isothermal titration calorimetry (ITC) was used to determine K_Ds for phosphorylated metabolites (SI figure 1, SI Table 2). A fluorescence assay, that measures the free Mg^{2+} concentration in a sample using the metal ion binding dye 8-Hydroxy-5-quinolinesulfonic (HQS) acid, was

used to estimate the K_D for Mg^{2+} metabolites that did not produce enough heat on binding to measure with ITC (SI figure 2, SI Table 3). For the HQS assay, Mg^{2+} is titrated into HQS solutions in the absence and presence of chelators. HQS emission as a function of the total Mg^{2+} in the absence of chelators is then fit to a binding model (SI figure 2A, top blue data and black fit). The free Mg^{2+} concentration is then then calculated from the fluorescence emission for each data point using the binding model, providing the free Mg^{2+} concentration as a function of the total Mg^{2+} concentration (SI figure 2B, bottom). Mg^{2+} binding by metabolites is thus observed by fitting the free Mg^{2+} concentration as a function of the total Mg^{2+} concentration, which is shifted to the right as Mg^{2+} is sequestered by metabolites.

The four nucleotide triphosphates, ATP, UTP, GTP, and dTTP, were classified as strong Mg^{2+} binders, with K_D values less than the approximate free Mg^{2+} concentration in *E. coli,* 2 mM (Table 1). Conversely, 8 other metabolites, L-glutamic acid, fructose 1,6-BP, UDP-N-acetylglucosamine, Glucose 6-phosphate, L-aspartic acid, 6-Phospho-gluconic acid, dihydroxyacetone phosphate, and pyruvic acid were classified as weak Mg^{2+} binders, with a K_D value greater than 2 mM (Table 1). Three metabolites, glutathione, L-valine, and L-glutamine had negligible Mg^{2+} binding properties, as measured with HQS (SI figure 2). We thus broke Eco80 down into two other artificial cytoplasms, NTP chelated Mg^{2+} (NTPCM), and weak metabolite chelated Mg^{2+} (WMCM), composed of the strong Mg^{2+} chelators (nucleotide triphosphates), and weak Mg^{2+} chelators, respectively (Table 1).

We next used two methods to estimate how the metabolites effect the speciation of free and chelated Mg^{2+} as a mixture. The first method was experimental, using HQS emission to estimate the free Mg^{2+} concentration in the presence of metabolites (Figure 1B-C, SI Table 3). The second method was a statistical model that accounts for experimental uncertainties in metabolite concentrations and uncertainty in K_D determination, based on single-site binding (meaning that one metabolite associates one Mg^{2+}). The statistical model is described in detail in the Supplementary Methods. Briefly, concentration errors were propagated from uncertainties in reagent masses and volumes used during sample preparation, and K_D uncertainties were obtained from the fits (Table 1). Both uncertainties were then randomly seeded into Equation 1 to create 1000 virtual artificial cytoplasms, where $[Mg]_T$ is the total Mg^{2+} concentration, [Mg] is the free Mg^{2+} concentration, i is an integer representing each metabolite in a mixture, N is the total number of metabolites in a mixture, $[L_i]_T$ is the concentration of a metabolite in a mixture, and K_D is the disassociation constant.

$$[Mg]_T = [Mg] + \sum_{i=1}^{N} \frac{[L_i]_T [Mg]}{K'_{Di} + [Mg]} \qquad (10)$$

Then, equation 1 is solved numerically to determine the free Mg^{2+} concentration produced at a given total Mg^{2+} concentration, in a virtual artificial cytoplasm.

The two methods indicate that Mg^{2+} speciates in artificial cytoplasms according to a single-site model within or below the biological free Mg^{2+} range of 0.5 to 3 mM Mg^{2+}, but not at higher free Mg^{2+} concentrations (Figure 1 E-F). For example, in Eco80, the statistical model suggests that the free Mg^{2+} should increase slowly as the total Mg^{2+} concentration is increased, until the strong Mg^{2+} chelators (NTPs) become saturated at about 27 mM total Mg^{2+} (Figure 1E, hex bins). At total Mg^{2+} concentrations higher than 27 mM, the free Mg^{2+} should increase faster because the NTPs are saturated by Mg^{2+} and the weak chelators sequester less Mg^{2+}. Free Mg^{2+}, calculated using HQS emission shows a similar trend to the statistical model below 3 mM Mg^{2+} free (Figure 1E, data points). However , the free Mg^{2+} concentration calculated from HQS emission does not increase with the total Mg^{2+} as fast as the single-site model would predict above 3 mM free Mg^{2+}, indicating that multivalent interactions, where one metabolite interacts with several Mg^{2+} molecules, dominate the equilibrium. Non-single-site behavior above 3 mM free Mg^{2+} is also observed in the NTPCM and WMCM artificial cytoplasms (Figure 1 F & G).

Lastly, we sought to empirically determine how much total Mg^{2+} is required to maintain a free Mg^{2+} concentration of 2 mM in Eco80, NTPCM, and WMCM. The relationship between the free Mg^{2+} calculated from HQS emission and the total Mg^{2+} concentration was fit to a polynomial to empirically approximate the data (Figure 1 E-G, colored lines), and the total Mg^{2+} concentration required to produce 2 mM Free Mg^{2+} was calculated from the polynomial fit. This resulted in a predicted 31.6, 25.0, and 6.5 mM total Mg^{2+} concentration to produce 2 mM free Mg^{2+} in Eco80, NTPCM, and WMCM, respectively (Table 2).

Eco80 destabilizes RNA helices

Paragraph 1: Transition

We sought to understand how Eco80 effects the stability of RNA helices composed of Watson-Crick base pairs.

Could not use the traditional method for thermodynamics, absorbance melting curves because of the high absorbtivity of ATP, UTP, GTP, dTTP, and UDP-N-acetylglucosamine.

Used fluorescence binding isotherms because the method is orthogonal to the optical properties of metabolites.

Paragraph 2: Fluorescence isotherms-intro

Described layout of assay, reagent conc, temperature control, expected results (Figure 2A)

Describe dependence of temperature and fit (Figure 2B)

Describe how the Van't hoff plot can be used to extract thermodynamic parameters

Paragraph 3: MeltR

Raw fluorecence was fit with a new program called MeltR to determine thermodynamic parameters

MeltR handles two sources of experimental error that can effect results: (1) uncertainties in RNA concentration determination and (2) inacurate K_Ds collected at low and high temperatures.

Paragraph 4: MeltR concentration optimization algorithm

Fit quality is highly dependent in the determination of RNA concentration, which is uncertain because of diextinction coefficient uncertainty, but errors are propagated systematically (SI Figure 3)

For example consider modeled data, assuming perfect data (SI Figure 4 A, left panel)

Now consider modeled data with +20% seeded error (SI Figure 4 A, middle panel)

Use low temperature isotherm to determine the correct R.

Will find the accurate dG even with 50% error in concentration determination.

Paragraph 5: MeltR only fits data from the most accurate isotherms

sffkpksdfpksd[pfk'[sdlk

Eco80 protects RNA from degradation